Mathematical Biology and Bioinformatics
2023. V. 18. № S. P. t1–t16. doi: 10.17537/2023.18.t1

Ttranslation of the original article
Trusov P.V. et al. Mathematical Biology and Bioinformatics. 2021;16(2):349–366.
doi: 10.17537/2021.16.349

================= **TRANSLATIONS OF PUBLISHED ARTICLES** =================

Mathematical Model of Airflow and Solid Particles Transport in the Human Nasal Cavity

Trusov P.V.[1,2], Zaitseva N.V.[1], Tsinker M.Yu.[*1,2], Nekrasova A.V.[2]

[1]*Federal Scientific Center for Medical and Preventive Health Risk Management Technologies, Perm, Russia*
[2]*Perm National Research Polytechnic University, Perm, Russia*

Abstract. As part of the mathematical model of the human respiratory system, a submodel is considered for the study of the non-steady airflow with solid particles (suspended particulate matter (PM) / dust particles) and the deposition of particles of various sizes in the human nasal cavity. It is assumed that the nasal cavity is divided by the bone-cartilaginous septum into two symmetrical (relative to the nasal septum) parts; the average geometry of the right part of the human nasal cavity is considered. The inhaled air is considered as a multiphase mixture of homogeneous single-component gas and solid dust particles. The Euler–Lagrange approach to modeling the motion of a multiphase mixture is used: a viscous liquid model is used to describe the motion of the carrier gas phase; the carried phase (dust particles) is modeled as separate inclusions of various sizes. The process of heating the inhaled air due to its contact with the walls is also taken into account. The features of the unsteady flow of a multiphase air mixture with dust particles were obtained using Ansys CFX for several scenarios. It has been noted that when studying the airflow in the nasal cavity, it is necessary to take into account the presence of turbulence, for which it is proposed to use the k-ω model. The velocity fields of inhaled air in the nasal cavity have been obtained; presented temperature distributions in the nasal cavity at different time points; made estimates of air heating at different temperatures of inhaled air; gave estimates of the proportion of deposited particles in the nasal cavity depending on the particle size for real machine-building production; presented trajectories of movement of suspended particles. Thus, it is shown that more than 99.7 % of particles with a diameter of more than 10 microns deposit in the human nasal cavity; as the particle diameter and mass decrease, the proportion of deposited particles decreases. Suspended particles with a size of less than 2.5 microns almost do not deposit in the nasal cavity. They can penetrate deeper into the lower airways and lungs of a person with the inhaled air and, having fibrogenic and toxic effect, can cause diseases. The results obtained are in good agreement with the results of individual studies performed by other scientists. Further development of the model involves studying airflow in the human lungs and modeling the formation of diseases caused by the harmful effects of environmental factors (including dust particles) entering the human body by inhalation.

Key words: *mathematical modeling, human respiratory system, nasal cavity, gas dynamics, suspended particles, dust particles, particulate matter, PM10, PM2.5, deposition, air heating.*

[*]cinker@fcrisk.ru

INTRODUCTION

Ambient air pollution with chemicals and dust particles produces negative effects on human health as evidenced in research works [1, 2], the respiratory system included [3–6]. The relevance of the issue has been outlined in the 'Clean Air' Federal project[1,2]. It has been implemented by the RF Government in 2019–2024 within the 'Ecology' National project and is aimed at reducing ambient air pollution in large industrial centers.

Up-to-date diagnostic methods can provide qualitative health assessment only during examination [7, 8] whereas use of mathematical models gives experts and decision-makers a possibility to make long-term predictions of how health would change under various environmental exposures. Our research team from the Federal Scientific Center for Medical and Preventive Health Risk Management Technologies has been developing a multi-level mathematical model for investigating how functional disorders develop in organs and systems of the human body depending on exposure to environmental factors [9].

We are developing a comprehensive meso-level model of the respiratory system to consider how environmental factors influence health under inhalation exposure [10], a model of the digestive systems aims to investigate oral exposures [11]; a model of the immune and neuroendocrine regulation is being developed to investigate protection mechanisms of the human body [12].

Within creating the aforementioned meso-level model of the respiratory system, we are developing sub-models of airflow in the large airways (upper and lower ones) and the human lungs. Airflow with solid particles and particle deposition in the large lower airways (the trachea and the first three generation of bronchi) was considered in our previous study [13]. Approaches to simulating airflow in the lungs are described in [14]. The upper airways perform some vital protective functions: they warm up inhaled air and purify it from dust particles that should be taken into account in models describing development of a disease. Therefore, it is necessary to investigate processes that occur in the upper airways. Such investigations become even more relevant due to new developing techniques of drug delivery by inhalation as well as due to up-to-date trends to use preliminary results of 'virtual operations' obtained with numerical methods and mathematical models prior to actual surgeries.

Air warming and purification is possible due to the complex anatomy of the nasal cavity. Air passes through the nasal cavity, which is a curved net of channels with variable cross-sections, numerous ledges and bumps. While passing through it, air contacts the nasal cavity walls, gets warmed and comes to the lower airways being warmer to prevent diseases in them. Dust particles occurring in inhaled air come into a contact with the nasal cavity mucosa and are halted there; they do not penetrate the lungs and are later excreted from the body.

Three-dimensional gas dynamics models are widely used to simulate airflow in the nasal cavity. Contemporary studies consider actual geometric shapes created by suing computer tomography. It is noteworthy that even if the overall structure of the nasal cavity is similar in all people, some peculiar shapes of it are quite different in different people. Thus, in the work [15], the authors provide 25 images of the nasal cavity with some unique features; the images were used to create average (standardized) geometry of the nasal cavity of a healthy person. This geometry was then used to investigate airflow in the nasal cavity. In the study [16], the authors simulated airflow in the nasal cavity of 30 adults; they reported 'extreme variety of shapes and, consequently, substantial differences in the airflow structure'.

Several studies by Russian researchers deserve special attention such as investigations accomplished by research teams from Novosibirsk (V.M. Fomin, V.L. Ganimedov,

[1] The RF President Order issued on May 07, 2018 No. 204 On national goals and strategic tasks of the development of the Russian Federation for the period up to 2024.

[2] The RF President Order issued on July 21, 2020 No. 474 On national goals of the development of the Russian Federation for the period up to 2030

M.I. Muchnaya and others) [16–19] and from Saint Petersburg (G.N. Lukyanova, A.A. Voronina, R.V. Neronova and others) [20–22]. These studies considered real three-dimensional shapes of the human nasal cavity based on tomography images; the authors investigated influence of different nasal cavity shapes on airflow distribution [16, 21]; considered stationary/quasi-stationary [16–19] and non-stationary statements [22]; reported statements and solutions with assumptions on both gas incompressibility [16–19] and compressibility [20, 22]; considered airflow turbulence [16, 17, 20–22]; investigated air warming [16, 20–22]; created numeric models to describe outcomes of surgeries [18, 21].

Airflow with sold particles in the human nasal cavity has been investigated in fewer studies by Russian researchers. Thus, the study [19] investigated gas suspension flow in stationary and non-stationary statements and considered laminar flow of an incompressible gas. The issue has been thoroughly investigated in foreign studies. The Euler–Lagrange approach is generally used in modeling [23–25]; usually, spherical particles are considered. Thus, the study [25] focused on airflow with particles and deposition of particles sized 1–30 μm; airflow with particles sized 1–100 nm was investigated in the study [24]. Particles with a diameter bigger than 10 μm are effectively deposited in the upper airways whereas smaller particles are able to penetrate the lower airways.

Airflow can be both laminar and turbulent depending on respiration (airflow rate) and individual features of the nasal cavity shape [26–28]. In case airflow rate is lower than 15 l/min, airflow is laminar; if it is higher than 20 l/min, airflow is turbulent [29–34]. When simulating airflow in the nasal cavity, many researchers report the necessity to consider turbulence; the studies [17, 18, 35, 36] reported using the k-ω model; [37], the k-ε model; [20, 22, 23], DES (detached eddy simulation).

Therefore, the present study is accomplished within the general goal, which is to develop the meso-level submodel of the human respiratory system. In this study, specific attention is paid to investigating non-stationary turbulent airflow with solid particles in the nasal cavity allowing for air warming and deposition of particles with various sizes.

CONCEPTUAL STATEMENT

Inhaled air is considered a gas suspension, that is, a multi-phase mixture of a homogenous one-phase gas and solid dust particles. We apply the Euler–Lagrange approach to simulate multi-phase mixture motion. The viscous flow model is applied to describe motion of a carrier gas phase; a carried phase (dust particles) is simulated as separate admixtures of various sizes. The k-ω model is used to consider turbulence since it has been established to be quite relevant for modeling internal flows along curved channels with small volumes and makes it possible to calculate near-wall turbulence.

Generally, dust particles can have different shapes (Figures 1,a and 1,b provide enlarged photos of dust particles emitted by civil engineering productions; the photos have been taken by experts from the Federal Scientific Center for Medical and Preventive Health Risk Management Technologies [38]). In this study, dust particles are assumed to be spherical. Particle velocity is equal to gas velocity at the entry cross-section.

The nasal cavity is divided into two halves (the right and the left) by the nasal septum made of the bone and cartilage. Both halves have similar structure and are almost symmetrical relative to the nasal septum. The nostril is the entry to each half of the nasal cavity. Air passes through it and comes to the front section in the nose (vestibule). Leaving the vestibule, air moves along three nasal passages (upper, middle and lower one) created by the superior, middle, and inferior nasal conchae, which are long, narrow, curled shelves of bone. After leaving the nasal passages, air comes into one common channel; its exit is called choana. It is the opening between the nasal cavity and the nasopharynx.

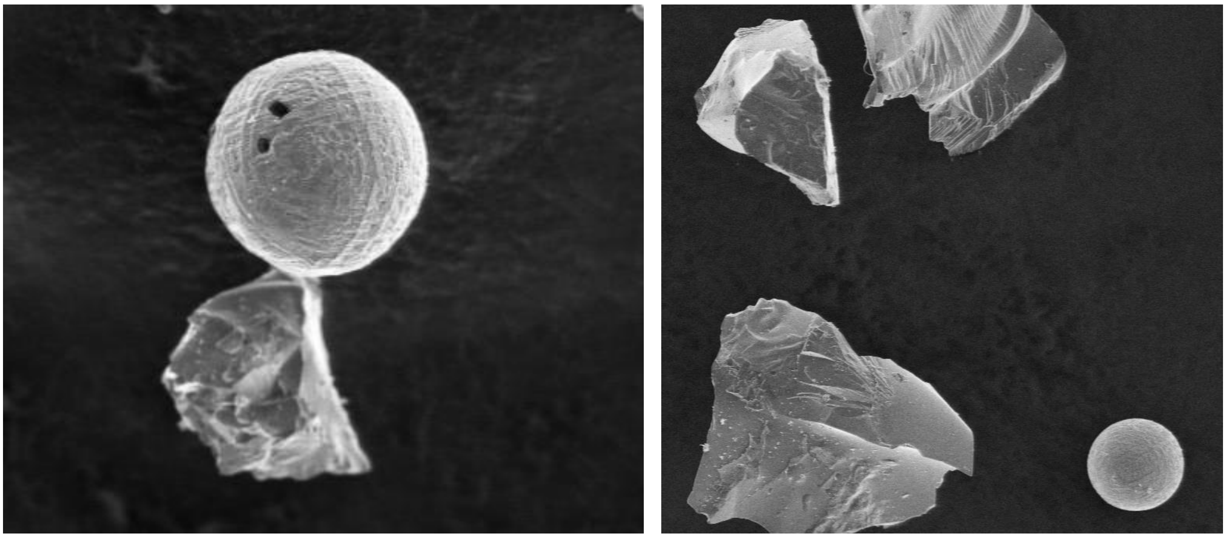

а)　　**б**)

Fig. 1. Photos of dust particles in emissions from civil engineering productions (a cutting-off machine) (magnification x300) [38].

Our aim was to identify properties of airflow with dust particles in it in the human nasal cavity. To do that, we used the standardized geometry of the nasal cavity based on tomography images of 30 healthy people without any anatomic anomalies. Images of the left nasal passages were mirrored relative to the symmetry plane thereby providing 30 additional sets of images showing the right nasal passages. A team of authors from Canada (Liu Y., Johnson M.R., Matida E.A., and others) obtained a standardized geometry of the right part of the human nasal cavity using 60 sets of images (the right and mirrored left ones) and a specific algorithm [39].

The surface mesh of the standardized nasal cavity (in .stl format) was kindly provided to us by Professor M.R. Johnson. Figure 2 shows the three-dimensional geometry of the human nasal cavity (right half) obtained by using the provided data and ANSYS ICEM CFD package.

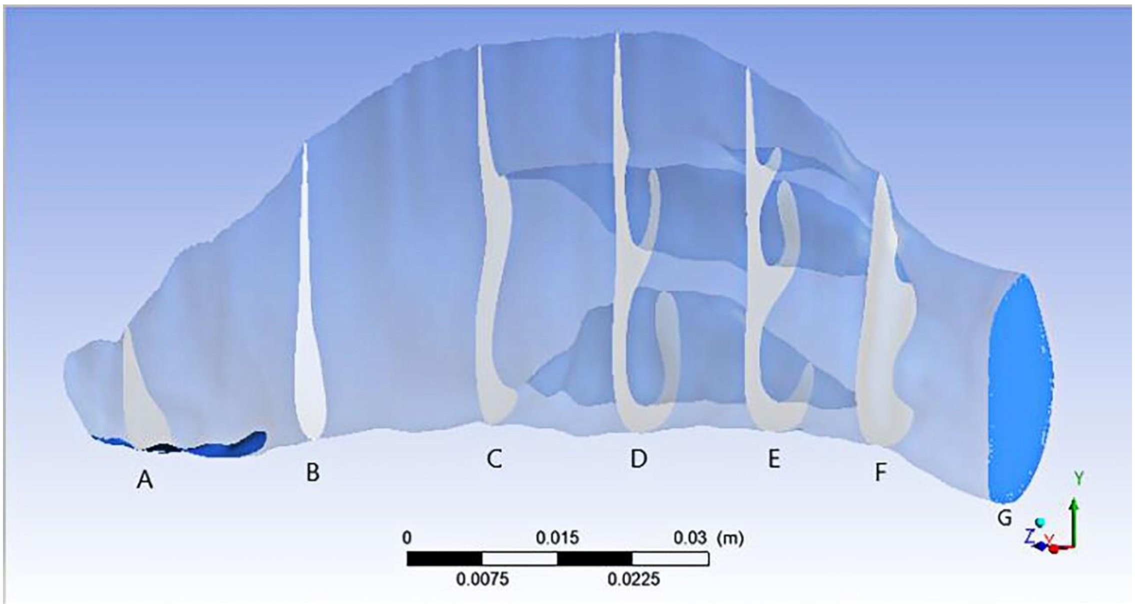

Fig. 2. The standardized three-dimensional geometry of the human nasal cavity (the right half).

The entry and exit zones are colored blue in Figure 2. We consider non-stationary airflow that occurs due to difference in pressure at the entry (the nostril, the area to the left in

Figure 2) and the exit (the choana, the cross-section G) in the nasal cavity. In Figure 2, the area to the left of the coronary cross-section C corresponds to the nasal vestibule; the area between the cross-sections C and F corresponds to the nasal passages (you can see the middle and lower nasal passages in the cross-section D and all three passages in the cross-section E). The constant atmospheric pressure is set at the entry to the nasal cavity ($p^{\text{atm}} = 101325$ Pa). The law of pressure change is set at the exit $p^{\text{out}} = 101325 - 98\sin(\frac{\pi}{2}t)$, tangential components of the stress tensor are assumed equal to zero both at the entry and the exit. Inhalation lasts two seconds ($t \in [0;2]$).

The nasal cavity walls are made of bones and hyaline cartilages; therefore, they are assumed to be solid and motionless. The mucosa and submucosa layer are covered with many venous vessels that make for air warming [40]. The constant temperature $\theta_\Gamma = 36.6$ °C is fixed at the nasal cavity walls; inhaled air contacts the walls and is warmed as it moves along the cavity. The surface of the nasal cavity walls is assumed to be covered with a highly viscous layer; suspended particles contact a wall, slow down and are halted. At the initial moment of time, pressure in the nasal cavity is equal to the atmospheric air pressure and temperature is 36.6 °C.

3. MATHEMATICAL STATEMENT

The mathematical statement of the problem to describe a flow of a multi-phase mixture containing a gas and solid particles has relationships for the carrier and carried phases, initial and boundary conditions. To describe motion of the gas (carrier) phase (labeled with the subscript (1)), we apply the following equations and relationships:

— the equation of continuity

$$\frac{\partial \rho_{(1)}}{\partial t} + \nabla \cdot (\rho_{(1)} \mathbf{v}_{(1)}) = 0; \tag{1}$$

— the equation of motion

$$\frac{\partial}{\partial t}(\rho_{(1)} \mathbf{v}_{(1)}) + \nabla \cdot (\rho_{(1)} \mathbf{v}_{(1)} \mathbf{v}_{(1)}) = \nabla \cdot \boldsymbol{\sigma}_{(1)} + \rho_{(1)} \mathbf{g} - \sum_j \mathbf{P}_{(1)(j)}; \tag{2}$$

— the relationship for the Cauchy stress tensor

$$\boldsymbol{\sigma}_{(1)} = -p_{(1)} \mathbf{I} + \boldsymbol{\tau}_{(1)}; \tag{3}$$

— the relationship for the deviator of the Cauchy stress tensor

$$\boldsymbol{\tau}_{(1)} = \eta_{(1)} (\boldsymbol{\nabla} \mathbf{v}_{(1)} + (\boldsymbol{\nabla} \mathbf{v}_{(1)})^T - \frac{2}{3} \mathbf{I} \boldsymbol{\nabla} \cdot \mathbf{v}_{(1)}); \tag{4}$$

— the energy conservation law

$$\frac{\partial}{\partial t}(\rho_{(1)} h_{\text{tot}}) - \frac{\partial p_{(1)}}{\partial t} + \nabla \cdot (\rho_{(1)} \mathbf{v}_{(1)} h_{\text{tot}}) = \nabla \cdot (\lambda \nabla \theta_{(1)}) + \nabla \cdot (\mathbf{v}_{(1)} \cdot \boldsymbol{\tau}_{(1)}); \tag{5}$$

— the relationships for kinetic energy of the k-ω model turbulence

$$\frac{\partial}{\partial t}(\rho_{(1)} k) + \nabla \cdot (\rho_{(1)} \mathbf{v}_{(1)} k) = \nabla \cdot (\mu + \frac{\mu_t}{\sigma_k} \nabla k) + P_k - \beta' \rho_{(1)} k \omega; \tag{6}$$

— the relationship for the specific energy dissipation rate of the k-ω model turbulence

$$\frac{\partial}{\partial t}(\rho_{(1)}\omega)+\nabla\cdot(\rho_{(1)}\mathbf{v}_{(1)}\omega)=\nabla\cdot(\mu+\frac{\mu_t}{\sigma_w}\nabla\omega)+\alpha\frac{\omega}{k}P_k-\beta\rho_{(1)}\omega^2\,; \tag{7}$$

— the equation of state for the hydrostatic component of the Cauchy stress tensor

$$p_{(1)}=\rho_{(1)}R\theta_{(1)}\,; \tag{8}$$

where $\rho_{(1)}$ is the density of air (the carrier phase), kg/m^3; $\mathbf{v}_{(1)}$ is the velocity vector of the carrier phase, m/s; $\boldsymbol{\sigma}_{(1)}$ is the Cauchy stress tensor of the carrier phase, Pa; $\mathbf{g}$ is the body force vector, m/s^2; $\mathbf{P}_{(1)(j)}$ is the member that describes the intensity of impulse exchange between the first and j-th phases, N/m^3; $p_{(1)}$ is the carrier phase pressure, Pa; $\mathbf{I}$ is the identity tensor; $\boldsymbol{\tau}_{(1)}$ is the deviator of the Cauchy stress tensor for the carrier phase, Pa; $\eta_{(1)}$ is the shear velocity of the carrier phase, Pa·s; h_{tot} is the total specific enthalpy, J; λ is the coefficient of thermal conductivity, W/(m·K); $\theta_{(1)}$ is the carrier phase temperature, °C; k is kinetic energy of turbulence, J/kg; μ is dynamic viscosity, Pa·s; μ_t is turbulent viscosity, Pa·s; P_k is the member that describes how turbulence occurs due to viscous forces; ω is the specific dissipation rate of turbulence energy; α, β, β', σ_k, σ_w is the turbulence model parameters ($\sigma_k=1, \sigma_w=2$).

The motion of solid particles (the carried phase, $j=\overline{2,J}$) is described with the following equations and relationships:

— the equations for identifying the travel velocities of the center of gravity for the j-th particle

$$\mathbf{v}_{(j)}=\frac{d\mathbf{r}_{(j)}}{dt}, \tag{9}$$

— the equations for motion of particles

$$m_{(j)}\frac{d\mathbf{v}_{(j)}}{dt}=\frac{1}{8}\rho_{(j)}\pi d_{(j)}^2 C_D\left|\mathbf{v}_{(1)}-\mathbf{v}_{(j)}\right|(\mathbf{v}_{(1)}-\mathbf{v}_{(j)})+m_{(j)}\mathbf{g}, \tag{10}$$

— the relationship for the coefficient of resistance to airflow for spherical particles

$$C_D=\begin{cases}\dfrac{24}{\mathrm{Re}}(1+0.15\,\mathrm{Re}), & if\ \mathrm{Re}\le 1000,\\ 0.44, & if\ \mathrm{Re}>1000,\end{cases}\qquad \mathrm{Re}=\frac{\left|\mathbf{v}_{(1)}-\mathbf{v}_{(j)}\right|d_{(j)}}{\nu_{(1)}}. \tag{11}$$

where $\mathbf{v}_{(j)}$ is the velocity of the center of gravity for the j-th particle, m/s; $\mathbf{r}_{(j)}$ is the radius-vector of the j-th particle's center of gravity; $m_{(j)}$ is the mass of the j-th particle, kg ($m_{(j)}=\frac{\pi}{6}d_{(j)}^3\rho_{(j)}$); $\rho_{(j)}$ –is the density of the j-th particle, *kg*/m^3; $d_{(j)}$ is the diameter of the j-th particle; C_D is the resistance coefficient; Re is the Reynolds number.

The initial conditions for the system of equations are as follows ($\mathbf{r}\in\bar{\Omega}$):

$$\mathbf{v}_{(j)}(0,\ \boldsymbol{r})=\mathbf{0}, \tag{12}$$

$$p_{(1)}(0,\ \boldsymbol{r})=p^{\text{atm}}, \tag{13}$$

$$\theta_{(1)}(0,\ \boldsymbol{r})=36.6, \tag{14}$$

where Ω is the internal area of the nasal cavity; Γ is the boundary of the nasal cavity area (the wall); Γ^{in}, Γ^{out} are the boundaries of the entry to and exit from the nasal cavity; $\bar{\Omega} = \Omega \bigcup \Gamma \bigcup \Gamma^{\text{in}} \bigcup \Gamma^{\text{out}}$ is the closed area.

The initial conditions include the following relationships:

— the relationship for the stress tensor components at the entry (Γ^{in}) for the carrier gas phase

$$\mathbf{n} \cdot \boldsymbol{\sigma}_{(1)} \cdot \mathbf{n} = p^{\text{atm}}, \qquad \mathbf{n} \cdot \boldsymbol{\sigma}_{(1)} - (\mathbf{n} \cdot \boldsymbol{\sigma}_{(1)} \cdot \mathbf{n})\mathbf{n} = 0, \tag{15}$$

— the relationship for the stress tensor components at the exit (Γ^{out}) for the carrier gas phase

$$\mathbf{n} \cdot \boldsymbol{\sigma}_{(1)} \cdot \mathbf{n} = p^{\text{out}}, \qquad \mathbf{n} \cdot \boldsymbol{\sigma}_{(1)} - (\mathbf{n} \cdot \boldsymbol{\sigma}_{(1)} \cdot \mathbf{n})\mathbf{n} = 0, \tag{16}$$

— the relationship for the temperature at the nasal cavity walls (Γ)

$$\theta\big|_{\Gamma} = 36.6, \tag{17}$$

— the relationship for the carrier phase temperature at the entry to the nasal cavity (Γ^{in})

$$\theta_{(1)}\Big|_{\Gamma^{\text{in}}} = \theta^{\text{Air}}, \tag{18}$$

— the relationship for the velocity of the carrier gas phase at the nasal cavity wall (Γ) (the adhesion condition)

$$\mathbf{v}_{(1)}\big|_{\Gamma} = \mathbf{v}^{AW}, \tag{19}$$

— the relationship for the velocity of particles (the carried phase, $j = \overline{2, J}$) at the nasal cavity wall (Γ) (the adhesion condition)

$$\mathbf{r}_j = \mathbf{r}^{AW}, \qquad \mathbf{n} \cdot (\mathbf{v}_j - \mathbf{v}^{AW}) < 0, \tag{20}$$

where $\mathbf{v}^{AW}$ is the velocity vector of the nasal cavity wall.

4. RESULTS

Flow of a multi-phase mixture containing a gas and solid particles in the human nasal cavity was computed with the Ansys software. The volume mesh was based on the surface mesh of the standardized nasal cavity (right half) (in .stl format), which was kindly provided to us by Professor M.R. Johnson [39]. The mesh was created by using the ANSYS ICEM CFD package. The internal volume of the employed geometry (Fig. 2) equals 13.19 cm^3; the surface area is 90.69 cm^2; the nasal cavity length (the difference between the end right point and the end left point of the area as per the Z coordinate (Fig. 2)) is 11.2 cm. The created volume mesh has 311,996 finite elements.

We identified properties of non-stationary flow of a multi-phase mixture containing air and dust particles by using Ansys CFX for several scenarios. The first group of scenarios (the scenarios from 1 to 5) focused on investigating air warming in the human nasal cavity: we computed scenarios for different temperature of inhaled air θ^{Air} (25 °C; 10 °C; 0 °C; –10 °C; –25 °C) without solid particles.

The scenario 6 investigates flow of inhaled air with solid particles that have different sizes (their diameters vary between 0.01 and 800 μm) and deposition of dust particles in the nasal cavity. The analyzed dust is emitted at an actual civil engineering production; the inhaled air (the carrier phase temperature) is 25 °C. Civil engineering productions are widely spread and usually involve active dust formation at most sections of employed technological processes. We considered the disperse structure of dust occurring due to an operating cutting-off machine. This technological operation creates huge amounts of particles covered by the established hygienic standards (PM_{10}, $PM_{2.5}$)[3]. Thus, Table 1 provides the disperse structure of dust emissions created by a cutting-off machine; it was identified by the experts from the Federal Scientific Center for Medical and Preventive Health Risk Management Technologies [38]. Obviously, approximately 33% of particles are smaller than 10 μm (PM_{10}), including 7 % of them being smaller than 2.5 μm ($PM_{2.5}$); sizes of approximately 67 % of particles vary between 10 and 800 μm. We examined a concentration of suspended aluminum oxide within the hygienic standard for the total solid particles, namely, the maximum permissible single maximum concentration (single maximum MPC), which was equal to 0.5 mg/m^3 [3].

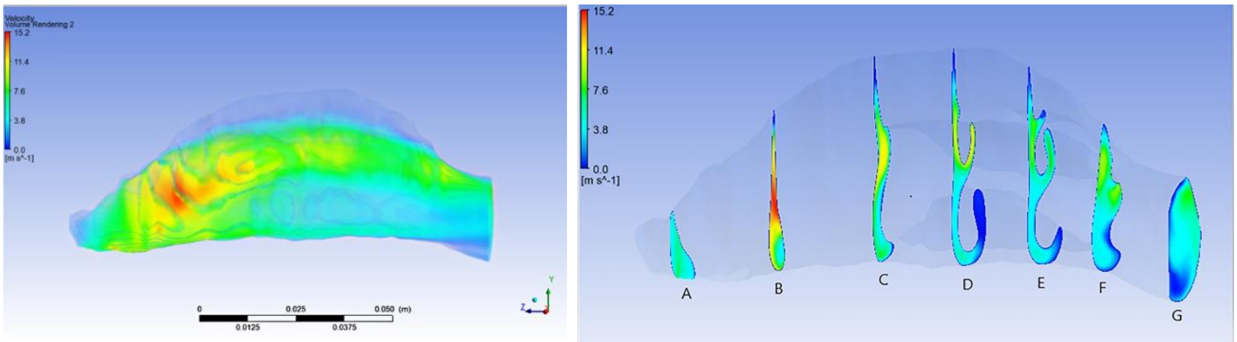

a) **b**)

Fig. 3. The field of airflow velocities at the time moment $t = 1$ (the scenario 1, $\theta^{Air} = 25$ °C): **a**) in the nasal cavity; **b**) in coronary cross-sections of the nasal cavity.

The airflow velocity changes within a range between 0 and 15 m/s during inhalation and reaches its peak at the time moment $t = 1$ (it corresponds to the middle of inhalation when the difference between pressure at the entry to and the exit from the nasal cavity is the greatest). Figure 3,a shows the field of airflow velocities at the time moment $t = 1$ (for the scenario 1 when the inhaled air temperature is $\theta^{Air} = 25$ °C); Figure 3,b shows the results in seven coronary cross-sections.

The greatest airflow velocity occurs in the nasal vestibule (the area between the coronary cross-sections B and C); airflow moves slower through the lower nasal passage than through the middle and upper ones. Figures 5,a–c show the fields of the velocity vector in three sagittal cross-sections (H, I, J) of the nasal cavity (shown in Fig. 4).

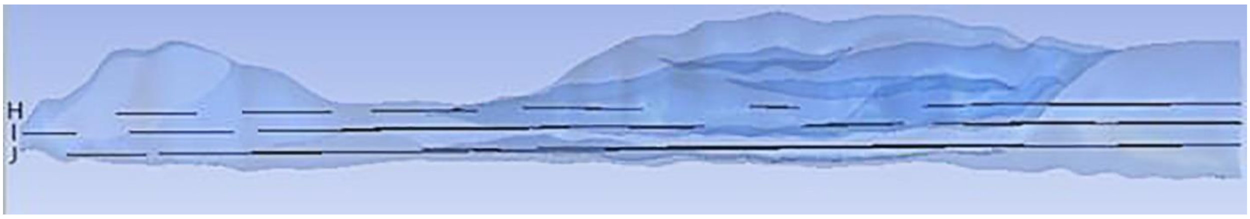

Fig. 4. The geometry of the human nasal cavity (the right half, top view).

[3] The hygienic standards HS 2.1.6.2604-10 Maximum permissible concentrations (MPC) of pollutants in ambient air in settlements. Appendix No. 8 to the HS 2.1.6.1338-03 approved in 2010 by the Order of the RF Chief Sanitary Inspector issued on April 19, 2010 No. 26.

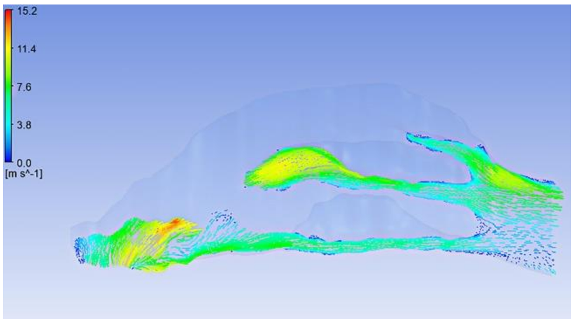

a)

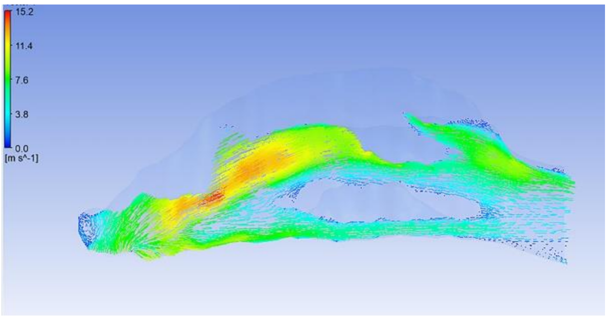

b)

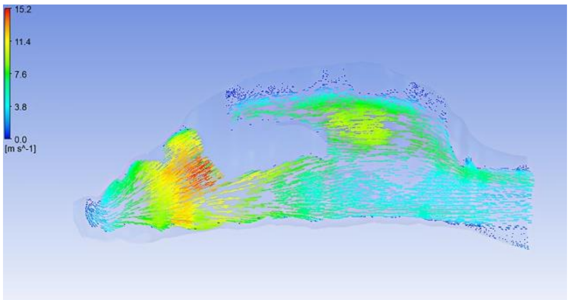

c)

Fig. 5. The velocity vector field ($\theta^{Air} = 25$ °C, $t = 1$ s): **a**) in the sagittal cross-section H; **b**) in the sagittal cross-section I; **c**) in the sagittal cross-section J.

As air flows through the nasal cavity, some vortexes occur; they facilitate air mixing and warming and protect from dust particles preventing their penetration deeper into the airways. Figure 6 shows some enlarged fragments of the nasal cavity where these vortexes occur: the enlarged fragment 1 (the nostril), 2 (the upper wall of the nasal valve), 3 (the superior or upper turbinate), 4 (the inferior or lower turbinate).

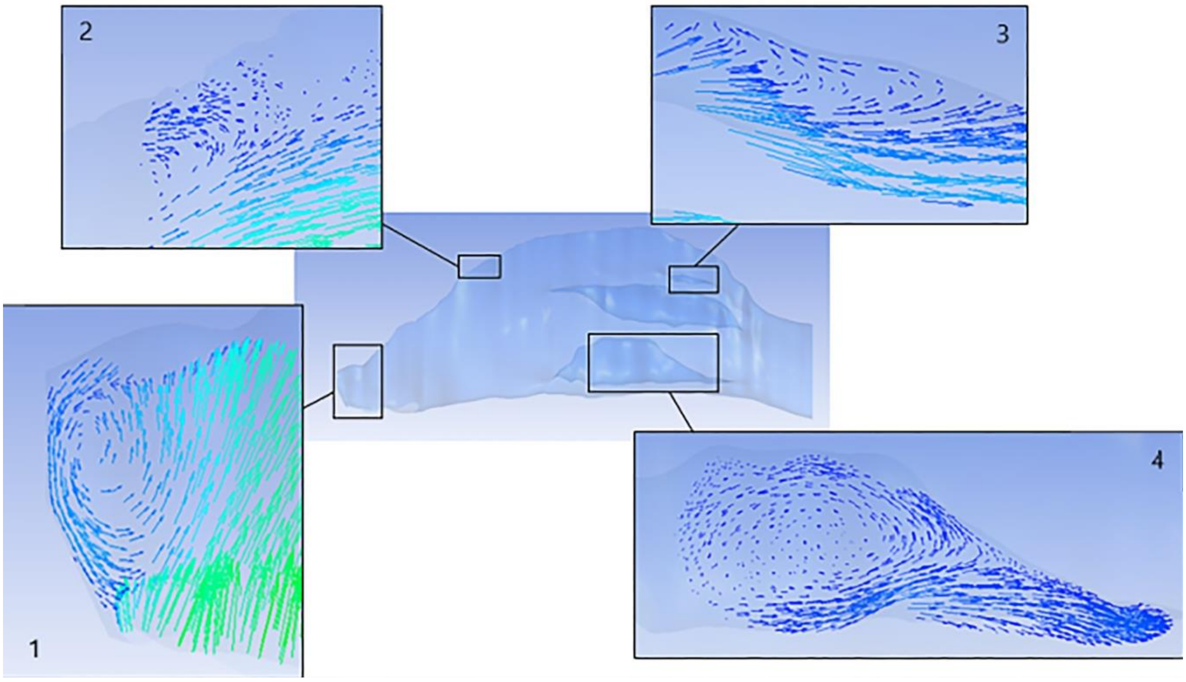

Fig. 6. The velocity vector field in the enlarged fragments of the nasal cavity.

Under the specified boundary conditions (the difference between the entry and exit pressure), the mass airflow rate reaches 0.0006 kg/s and the volume airflow rate is approximately 30 l/min. The Reynolds numbers equal approximately 3200 for such conditions; airflow involves occurrence of vortexes; airflow is turbulent in its essence.

Preliminary computations of airflow with turbulence and without it established significant differences in airflow properties. All the described scenarios were created using the *k*-ω turbulence model.

Examination of air warming

Inhaled air is warmed as it passes through the nasal cavity. Figures 7,a–e show the distribution of temperatures in the sagittal cross-section I of the nasal cavity during inhalation at different moments of time (0.1 s; 0.5 s; 1 s; 1.5 s; 2 s). The images are made for the scenario 1 when the temperature of inhaled air equals 25 °C.

In Figures 7,a–e, blue color corresponds to colder air and red color corresponds to warmer air. The lowest temperature is observed near the entry to the nasal cavity. As air goes deeper into the nasal cavity, its temperature grows and reaches its maximum value near the choana. The most intensive air warming occurs at the beginning and the end of inhalation (Fig. 7,a and 7,e). The airflow velocities are the lowest at these moments and air gets warmed more due to a longer contact with the nasal cavity walls. In the middle of inhalation (Fig. 7,b–d), inhaled air is warmed less intensely. Areas near the walls are warmed up to higher temperatures (they are painted red in Figures). Figure 8 provides temperatures at the exit from the nasal cavity during inhalation in the scenarios 1–5 that are different as per temperatures of inhaled air.

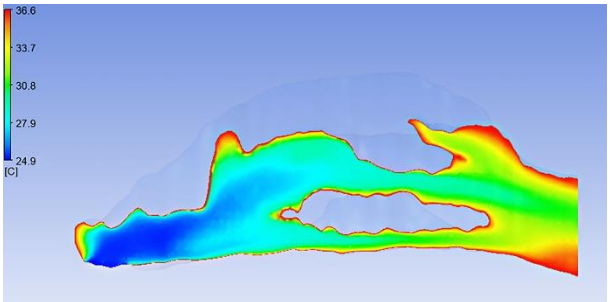

a)

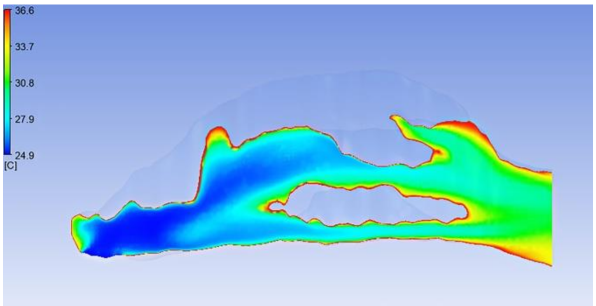

b)

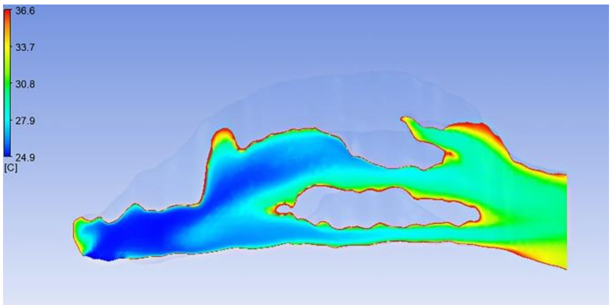

c)

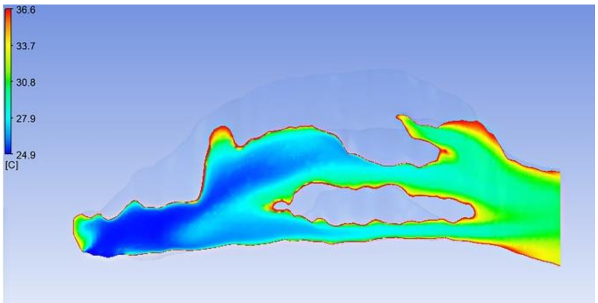

d)

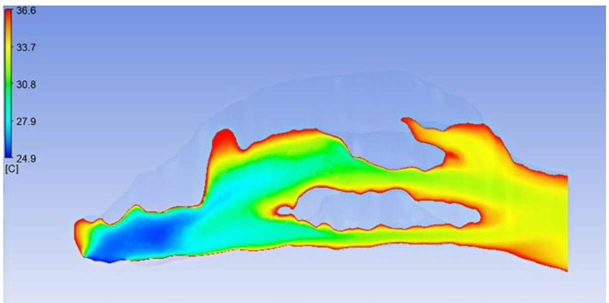

e)

Fig. 7. Distribution of temperatures in the sagittal cross-section I of the nasal cavity ($\theta^{Air} = 25$ °C) at different moments of time: **a**) $t = 0.1$ s; **b**) $t = 0.5$ s; **c**) $t = 1$ s; **d**) $t = 1.5$ s; **e**) $t = 2$ s.

The warmer inhaled air is at the initial moment, the higher temperature value is reached during inhalation. According to the results obtained by numeric modeling, if the inhaled air temperature is 25 °C, air is warmed up to 31.5–34.2 °C (Fig. 8) while passing through the nasal cavity; if the inhaled air temperature is 10 °C (θ^{Air} = 10 °C), air is warmed up to 24.5–31 °C; 0 °C, up to 20.3–28.5 °C; –10 °C; up to 15.3–26 °C; –25 °C; up to 8–22.5 °C.

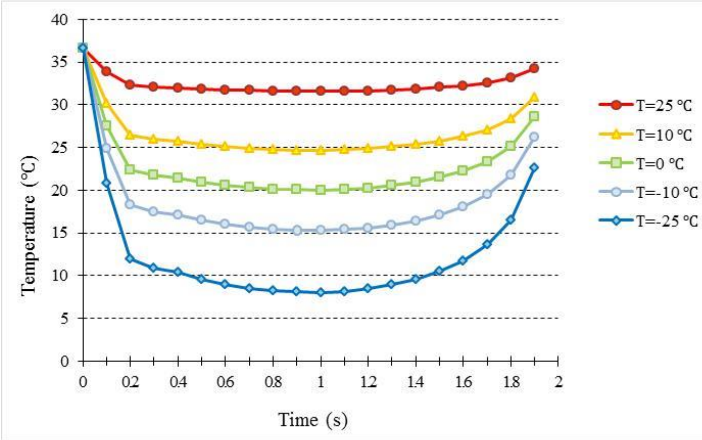

Fig. 8. Air temperature at the cross-section of the exit from the nasal cavity under different tempertures of inhaled air.

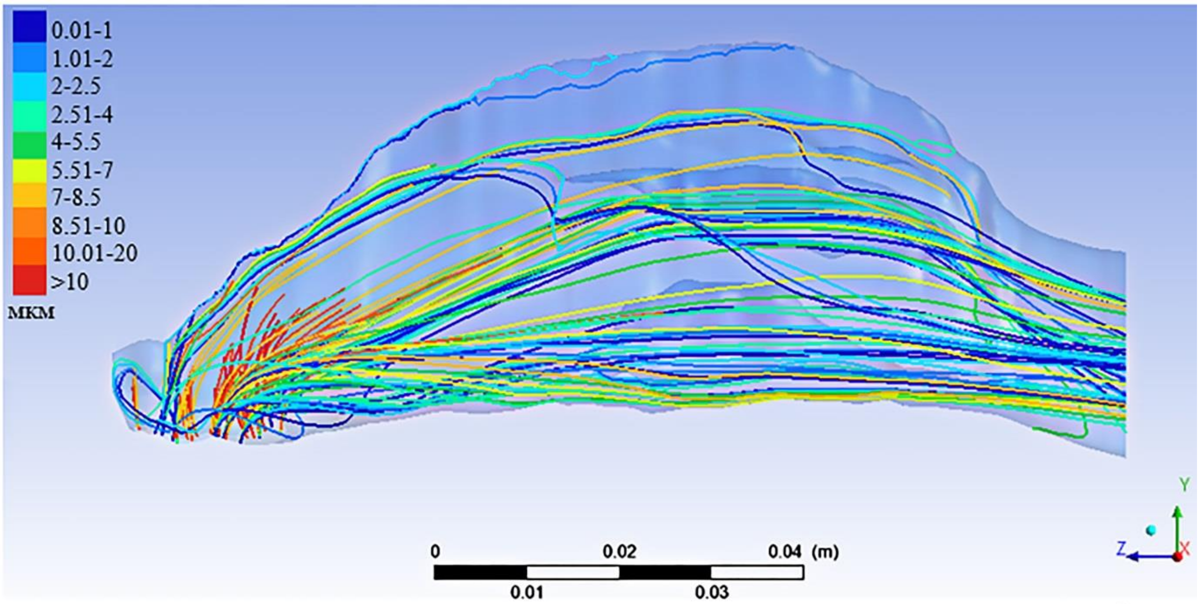

Fig. 9. Motion patterns of particles emitted by an operating cutting-off machine in the human nasal cavity.

Examination of particle deposition

The scenario 6 involved examining a flow of a multi-phase mixture containing air and solid particles emitted by an operating cutting-off machine at an actual civil-engineering production. Table 1 provides the disperse structure of dust emissions as per fractions employed in the model as well as a share of particles that are deposited in the nasal cavity according to numeric modeling results.

Table 1. The disperse structure of dusts emitted by an operating cutting-off machine; a share of particles deposited in the human nasal cavity established by numeric modeling

Particle size, μm		**Volume fraction of the total particle volume as per identified ranges, %**	**A share of deposited particles, % (numeric modeling results)**
Particle size > 10 μm	700.01–800.0	0.37	99.93 %
	600.01–700.0	–	–
	500.01–600.0	0.88	99.94 %
	400.01–500.0	4.54	99.92 %
	300.01–400.0	1.81	99.91 %
	200.01–300.0	2.71	99.94 %
	100.01–200.0	4.61	99.91 %
	90.01–100.00	–	–
	80.01–90.00	1.55	99.91 %
	70.01–80.00	1.93	99.94 %
	60.01–70.00	2.90	99.91 %
	50.01–60.00	4.07	99.91 %
	40.01–50.00	4.12	99.91 %
	30.01–40.00	5.80	99.93 %
	20.01–30.00	7.72	99.90 %
	10.01–20.00	24.04	99.71 %
PM_{10} (particle size is below or equal to 10 μm)	8.51–10.00	4.20	92.75 %
	7.01–8.50	4.56	80.87 %
	5.51–7.00	4.58	68.76 %
	4.01–5.50	6.78	47.31 %
	2.51–4.00	5.80	23.43 %
$PM_{2.5}$ (particle size ≤ 2.5 μm)	2.01–2.50	1.42	0.00 %
	1.01–2.00	3.39	0.00 %
	0.01–1.00	2.27	0.00 %

According to the results of numeric modeling, more than 99.7 % of particles with their size exceeding 10 μm are deposited in the nasal cavity and do not reach the nasopharynx (Table 1). This occurs because large particles with a substantially high mass tend to follow the inertia mechanisms of deposition. When the carrier phase sharply changes its direction, large particles go on moving in the previous direction, hit the nasal cavity mucosa and are deposited on it.

As particle sizes and diameters grow smaller, a share of deposited particles goes down; thus, only 92.75 % of particles sized 8.5–10 μm are deposited in the nasal cavity; 80.87 % of particles sized 7–8.5 μm; 68.76 % of particles sized 5.5–7 μm; 47.31 % of particles sized 4–5.5 μm; 23.43 % of particles sized 2.5–4 μm. According to numeric modeling results, solid particles $PM_{2.5}$ are hardly ever deposited in the nasal cavity. Figure 9 provides motion patterns of particles in the nasal cavity depending on their sizes.

Particles sized bigger than 10 μm have similar motion patterns. In Figure 9, all patterns with their diameter exceeding 10 μm are colored dark red. Almost all particles sized bigger than 10 μm are deposited in the nasal vestibule. Particles sized 7–10 μm (are colored orange tints) reach the nasal passages; smaller particles (are colored light or dark blue) reach the entry to the nasopharynx and penetrate the lower airways.

DISCUSSION

The research results are consistent with findings reported in some other studies. Thus, computed airflow velocities in the nasal cavity correspond to data reported in the works [17, 22]; volume flow rate and mass flow rate are well in line with the data described in the study [41].

Some vortexes occur when air flows through the nasal cavity; airflow is turbulent in its essence and due to this fact it is necessary to consider turbulence when modeling airflow just as it was established in the works [17, 18, 20, 22, 23, 26–37].

Our findings as regards air warming in the scenario 1 (the temperature of inhaled air is 25 °C and air is warmed up to 31.5–34.2 °C while passing through the nasal cavity) confirm the data obtained in the study [42], where inhaled air with its temperature being 25 °C is reported to be warmed up to 34 °C. Our data are also close to findings described in the study [43].

According to the results obtained by numeric modeling, particles sized bigger than 10 μm are effectively deposited in the nasal cavity and this is consistent with the established concepts [25, 24, 44, 45]. Thus, according to the study [25], a share of particles sized bigger than 10 μm that are deposited in the nasal cavity reaches 97 %; therefore, it is recommended to use aerosols with their disperse phase exceeding 8 μm to treat diseases of the nasal cavity. Suspended particles $PM_{2.5}$ are hardly ever deposited in the human nasal cavity; when carried by inhaled air, they are able to penetrate the lower airways and lungs. Since such particles can produce fibrogenic and toxic effects, they can cause diseases. When investigating effects produced by dust particles on human health, experts should pay special attention to particles sized smaller than 2.5 μm due to their ability to penetrate deeper into the human body.

CONCLUSION AND FUTURE PROSPECTS

Therefore, we have investigated non-stationary airflow with solid particles in the human nasal cavity within the development of the meso-level model describing the human respiratory system. We have considered air warming and depositions of particles with different sizes in the nasal cavity under several scenarios. It was noted that turbulence should be considered when investigating airflow in the nasal cavity.

In this study, we have obtained the fields of inhaled air velocities in the nasal cavity; we have described distribution of temperatures in the nasal cavity at different moments of time; we have estimated air warming under different temperatures of inhaled air; we have computed shares of particles deposited in the nasal cavity depending on their size; we have identified motion patterns for solid particles penetrating the body with inhaled air. The study also reports the results of numeric modeling aimed at describing inhaled air flow in the nasal cavity under exposure to dusts emitted by machinery at an actual civil engineering production. It was established that more than 99.7 % of particles sized bigger than 10 μm were deposited in the nasal cavity; particles sized smaller than 2.5 μm were hardly ever deposited in the nasal cavity.

The exit from the upper airways is simultaneously the entry to the lower ones. The results obtained by using this sub-model are input data in the sub-model that describes the lower airways and lungs. Further development of the model involves investigating airflow in the human lungs and modeling occurrence of diseases caused by exposure to harmful environmental factors able to penetrate the human body through inhalation.

REFERENCES

1. Brunekreef B., Holgate S.T. Air pollution and health. *Lancet*. 2002. V. 360. P. 1233–1242. doi: 10.1016/S0140-6736(02)11274-8
2. Zaitseva N.V., Ustinova O.Iu., Aminova A.I. *Gigienicheskie aspekty narusheniia zdorov'ia detei pri vozdeistvii khimicheskikh faktorov sredy obitaniia* (Hygienic aspects of children's health disorders under the influence of chemical factors of the environment). Ed. Zaitseva N.V. Perm', 2011. 489 p. (in Russ.).

3. Xing Y.-F., Xu Y.-H., Shi M.-H., Lian Y.-X. The impact of PM2.5 on the human respiratory system. *Journal of Thoracic Disease*. 2016. V. 8. No. 1. P. E69–E74. doi: 10.3978/j.issn.2072-1439.2016.01.19
4. Vlasova E.M., Vorobeva A.A., Ponomareva T.A. Peculiarities of cardiovascular pathology formation in workers of titanium-magnesium production. *Russian Journal of Occupational Health and Industrial Ecology*. 2017. V. 9. P. 38 (in Russ.).
5. Tikhonova I.V., Zemlyanova M.A., Kol'dibekova Yu.V., Peskova E.V., Ignatova A.M. Hygienic assessment of aerogenic exposure to particulate matter and its impacts on morbidity with respiratory diseases among children living in a zone influenced by emissions from metallurgic production. *Health Risk Analysis*. 2020. V. 3. P. 61–69. doi: 10.21668/health.risk/2020.3.07.eng
6. Vlasova E.M., Ustinova O.Yu., Nosov A.E., Zagorodnov S.Yu. Peculiarities of respiratory organs diseases in smelters dealing with titanium alloys under combined exposure to fine-disperse dust and chlorine compounds. *Hygiene and Sanitation*. 2019. V. 98. No. 2. P. 153–158 (in Russ.). doi: 10.18821/0016-9900-2019-98-2-153-158
7. Grebenev A.L. *Propedevtika vnutrennikh boleznei* (Propedeutics of Internal Medicine). Moscow, 2001. 592 p. (in Russ.).
8. Shkliar B.S. *Diagnostika vnutrennikh boleznei* (Diagnostics of internal diseases). Kiev, 1972. 516 p. (in Russ.).
9. Trusov P.V., Zaitseva N.V., Kiryanov D.A., Kamaltdinov M.R., Cinker M.Ju., Chigvintsev V.M., Lanin D.V. A Mathematical model for evolution of human functional disorders influenced by environment factors. *Mathematical Biology and Bioinformatics*. 2012. V. 7. No. 2. P. 589–610 (in Russ.). doi: 10.17537/2012.7.589
10. Trusov P.V., Zaitseva N.V., Tsinker M.Yu. Modeling of human breath: conceptual and mathematical statements. *Mathematical Biology and Bioinformatics*. 2016. V. 11. No. 1. P. 4–80 (in Russ.). doi: 10.17537/2016.11.64
11. Kamaltdinov M.R. 3D modeling of antroduodenal zone motility of digestive track for the purpose of health risks evaluation with peroral exposition to chemicals. *Health Risk Analysis*. 2014. V. 2. P. 68–75. doi: 10.21668/health.risk/2014.2.08.eng
12. Kiryanov D.A., Lanin D.V., Chigvintsev V.M. Mathematical model of immune and neuroendocrine systems functioning with regard to evolution of organ synthetic function violations. *Health Risk Analysis*. 2015. V. 3. P. 68–72. doi: 10.21668/health.risk/2015.3.10.eng
13. Trusov P.V., Zaitseva N.V., Tsinker M.Yu., Babuskina A.V. Modelling dusty air flow in the human resperatory tract. *Russian Journal of Biomechanics.* 2018. V. 22. No. 3. P. 301–314 (in Russ.).
14. Trusov P.V., Zaitseva N.V., Tsinker M.YU. On modeling of airflow in human lungs: constitutive relations to describe deformation of porous medium. *PNRPU Mechanics Bulletin*. 2020. V. 4. P. 165–174 (in Russ.). doi: 10.15593/perm.mech/2020.4.14
15. Brüning J., Hildebrandt T., Heppt W., Schmidt N., Lamecker H., Szengel A., Amiridze N., Ramm H., Bindernagel M., Zachow S., Goubergrits L. Characterization of the Airflow within an Average Geometry of the Healthy Human Nasal Cavity. *Scientific Reports*. 2020. V. 10. No. 1. P. 3755. doi: 10.1038/s41598-020-60755-3
16. Ganimedov V.L., Muchnaya M.I., Sadovskii A.S. Air flow in the human nasal cavity. Results of mathematical modelling. *Russian Journal of Biomechanics*. 2015. V. 19. No. 1. P. 31–44.
17. Fomin V.M., Vetlutsky V.N., Ganimedov V.L., Muchnaya M.I., Shepelenko V.N., Melnikov M.N., Savina A.A. Air flow in the human nasal cavity. *Journal of Applied Mechanics and Technical Physics*. 2010. V. 51. No. 2. P. 233-240. doi: 10.1007/s10808-010-0033-y
18. Sadovskii A.S., Bosykh L.Iu., Ganimedov V.L., Muchnaia M.I. In: *XI Vserossiiskii s''ezd po fundamental'nym problemam teoreticheskoi i prikladnoi mekhaniki* (The XI

All-Russian Congress on Basic Problems of Theoretical and Applied Mechanics): abstracts. 2015. P 3298–3300 (in Russ.).

19. Ganimedov V.L., Muchnaya M.I. Numerical simulation of particle deposition in the human nasal cavity. *Thermophysics and Aeromechanics*. 2020. V. 27. No. 2. P. 303–312. doi: 10.1134/S0869864320020122
20. Voronin A., Luk'yanov G., Neronov R. Computational modeling of airflow in nonregular shaped channels. *Scientific and Technical Journal of Information Technologies, Mechanics and Optics*. 2013. V. 3. No. 85. P. 113–118.(in Russ.).
21. Neronov R.V., Luk'yanov G.N., Rassadina A.A., Voronin A.A., Malyshev A.G. The effect of the nasal cavity form on air flow distribution during inhalation. *Russian Otorhinolaryngology*. 2017. V. 1. No. 86. P. 83–94 (in Russ.). doi: 10.18692/1810-4800-2017-1-83-94
22. Lukyanov G.N., Voronin A.A., Rassadina A.A. Simulation of convective flows in irregular channels on the example of the human nasal cavity and paranasal sinuses. *Technical Physics*. 2017. V. 62. No. 3. P. 484–489. doi: 10.1134/S1063784217030136
23. Tang H., Tu J.Y., Li H.F., Au-Hijleh B., Xue C.C., Li C.G. Dynamic Analysis of Airflow Features in a 3D Real-Anatomical Geometry of the Human Nasal Cavity. *15th Australasian Fluid Mechanics Conference*. Sydney, Australia, 2004. https://www.aeromech.usyd.edu.au/15afmc/proceedings/papers/AFMC00174.pdf (accessed 15.06.2021).
24. Zamankhan P., Ahmadi G., Wang Z., Hopke P.K., Cheng Y-S., Su W.S., Leonard D. Airflow and Deposition of Nano-Particles in a Human Nasal Cavity. *Aerosol Science and Technology*. 2006. V. 40. P. 463–476. doi: 10.1080/02786820600660903
25. Saghaian S.E., Azimian A.R., Jalilvand R. Dadkhah S., Saghaian S.M. Computational analysis of airflow and particle deposition fraction in the upper part of the human respiratory system. *Biology, Engineering and Medicine*. 2018. V. 3. No. 6. P. 6–9. doi: 10.15761/BEM.1000155
26. Doorly D.J., Taylor D.J., Gambaruto A.M., Schroter R.C., Tolley N. Nasal architecture: form and flow. *Philosophical Transactions of the Royal Society A: Mathematical, Physical and Engineering Sciences*. 2008. doi: 10.1098/rsta.2008.0083
27. Doorly D.J., Taylor D.J., Schroter R.C., Mechanics of airflow in the human nasal airways. *Respiratory Physiology and Neurobiology*. 2008. V. 163. P. 100–110. doi: 10.1016/j.resp.2008.07.027
28. Inthavong K., Das P., Singh N., Sznitman J. In silico approaches to respiratory nasal flows: A review. *Journal of Biomechanics*. 2019. V. 97. P. 109434. doi: 10.1016/j.jbiomech.2019.109434
29. Subramaniam R., Richardson R., Morgan K., Kimbell J., Guilmette R. Computational fluid dynamics simulations of inspiratory airflow in the human nose and nasopharynx. *Inhalation Toxicology*. 1998. P. 91–120. doi: 10.1080/089583798197772
30. Zhao K., Scherer P.W., Hajiloo S.A., Dalton P. Effect of anatomy on human nasal air flow and odorant transport patterns: Implications for olfaction. *Chemical Senses*. 2004. V. 29. No. 5. P. 365–379. doi: 10.1093/chemse/bjh033
31. Shang Y.D., Inthavong K., Tu J.Y. Detailed micro-particle deposition patterns in the human nasal cavity influenced by the breathing zone. *Computers and Fluids*. 2015. V. 114. P. 141–150. doi: 10.1016/j.compfluid.2015.02.020
32. Garcia G.J., Bailie N., Martins D.A., Kimbell J.S. Atrophic rhinitis: A CFD study of air conditioning in the nasal cavity. *Journal of Applied Physiology*. 2007. V. 103. P. 1082–1092. doi: 10.1152/japplphysiol.01118.2006
33. Ge Q.J., Inthavong K., Tu J.Y. Local deposition fractions of ultrafine particles in a human nasal-sinus cavity CFD model. *Inhalation Toxicology*. 2012. V. 24. No. 8. P. 492–505. doi: 10.3109/08958378.2012.694494

34. Goodarzi-Ardakani V., Taeibi-Rahni M., Salimi M.R., Ahmadi G. Computational simulation of temperature and velocity distribution in human upper respiratory airway during inhalation of hot air. *Respiratory Physiology and Neurobiology*. 2016. V. 223. P. 49–58. doi: 10.1016/j.resp.2016.01.001
35. Hörschler I., Brücker C., Schr¨oder W., Meinke M., Investigation of the impact of the geometry on the nose flow. *European Journal of Mechanics, B/Fluids*. 2006. V. 25. P. 471–490. doi: 10.1016/j.euromechflu.2005.11.006
36. Wen J., Inthavong K., Tu J., Wang S. Numerical simulations for detailed airflow dynamics in a human nasal cavity. *Respiratory Physiology and Neurobiology*. 2008. V. 161. P. 125–135. doi: 10.1016/j.resp.2008.01.012
37. Lindemann J., Brambs H.-J., Keck T., Wiesmiller K.M., Rettinger G., Pless D. Numerical simulation of intranasal airflow after radical sinus surgery. *American Journal of Otolaryngology – Head and Neck Medicine and Surgery*. 2005. V. 26. No. 3. P. 175–180. doi: 10.1016/j.amjoto.2005.02.010
38. Mai I.V., Zaitseva N.V., Ulanova T.S., Vekovshinina S.A., Zagorodnov S.Iu., Kokoulina A.A., Sedusova E.V., Popova E.V. *Atlas promyshlennykh pylei. Pyli mashinostroitel'nykh, metallurgicheskikh, gornodobyvaiushchikh, gorno-pererabatyvaiushchikh proizvodstv i predpriiatii tsvetnoi metallurgii* (Industrial dust atlas. Dust from engineering, metallurgical, mining, mining and processing industries and non-ferrous metallurgy enterprises). Perm', 2014. 285 p. (in Russ.).
39. Liu Y., Johnson M.R., Matida E.A., Kherani S., Marsan J. Creation of a standardized geometry of the human nasal cavity. *J. Appl. Physiol*. 2009. V. 106. P. 784–795. doi: 10.1152/japplphysiol.90376.2008
40. Borziak E.I., Volkova L.I., Dobrovol'skaia E.A., Revazov V.S., Sapin M.R. *Anatomiia cheloveka* (Human anatomy). Ed. M.R. Sapin. Moscow, 1993. Vol. 1. 544 p. (in Russ.).
41. Liu Y., Matida E.A., Johnson M.R. Experimental measurements and computational modeling of aerosol deposition in the Carleton-Civic standardized human nasal cavity. *Journal of Aerosol Science*. 2010. V. 41. P. 569–586. doi: 10.1016/j.jaerosci.2010.02.014
42. Inthavong K., Wen J., Tu J., Tian Z. From CT scans to CFD modelling-fluid and heat transfer in a realistic human nasal cavity. *Eng. Appl. Comput. Fluid Mech*. 2009. V. 3. No. 3. P. 321–335. doi: 10.1080/19942060.2009.11015274
43. Garcia J.M., Schroeter J.D., Kimbell J.S. Sniffing out airflow and transport processes in the nasal cavity. *Fluent News Appl. Comput. Fluid Dynamics*. 2006. V. 15. No. 3. P. 3–5.
44. Katsnel'son B.A., Alekseeva O.G., Privalova L.I., Polzik E.V. *Pnevmokoniozy: patogenez i biologicheskaia profilaktika* (Pneumoconiosis: pathogenesis and biological prevention). Ekaterinburg, 1995. 325 p.(in Russ.).
45. Brain J.D., Valberg P.A. Models of lung retention based on the ICRP task group report. *Arch. Environ. Health*. 1974. V. 28. No. 1. P. 1–11. doi: 10.1080/00039896.1974.10666424

Received 19.05.2023.
Published 08.07.2023.